# Nanoscale

Accepted Manuscript


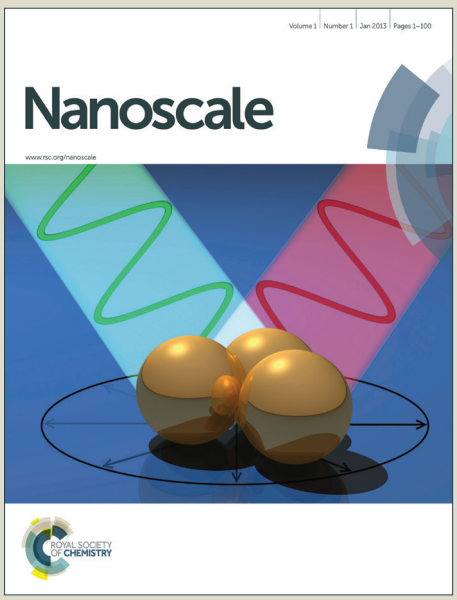





ROYAL SOCIETY OF CHEMISTRY

www.rsc.org/nanoscale

# Electronic transport in benzodifuran single-molecule transistors

An Xiang,[1,2,*] Hui Li,[3,*] Songjie Chen,[3] Shi-Xia Liu,[3,†] Silvio Decurtins,[3] Meilin Bai,[1] Shimin Hou,[1,‡] and Jianhui Liao[1,§]

[1]*Key Laboratory for the Physics and Chemistry of Nanodevices, Department of Electronics, Peking University, Beijing 100871, China*

[2]*Academy for Advanced Interdisciplinary Studies, Peking University, Beijing 100871, China*

[3]*Departement für Chemie und Biochemie, Universität Bern, Freiestrasse 3, 3012 Bern, Switzerland*

(Dated: March 15, 2015)

## Abstract

**Benzodifuran (BDF) single-molecule transistors have been fabricated in electromigration break junctions for electronic measurements. The inelastic electron tunneling spectrum validates that the BDF molecule is the pathway of charge transport. The gating effect is analyzed in the framework of single-level tunneling model combined with transition voltage spectroscopy (TVS). The analysis reveals that the highest occupied molecular orbital (HOMO) of the thiol-terminated BDF molecule dominates the charge transport through Au-BDF-Au junctions. Moreover, the energy shift of the HOMO caused by the gate voltage is the main reason of the conductance modulation. In contrast, the electronic coupling between the BDF molecule and the gold electrodes, which significantly affects the low-bias junction conductance, is only influenced slightly by the applied gate voltage. These findings will help in the design of future molecular electronic devices.**

**Keywords:** single-molecule transistor, energy level alignment, coupling, electromigration



*These two authors contributed equally to this work.

†Electronic address: liu@dcb.unibe.ch

‡Electronic address: smhou@pku.edu.cn

§Electronic address: Jianhui.Liao@pku.edu.cn

## Introduction

Design and construction of electronic devices using single or very few molecules as the active functional unit is a promising approach to further miniaturize electronic devices and also provides a versatile testbed for many basic quantum transport concepts [1–3]. Extensive experiments have demonstrated that the current through single molecules can be modulated by external stimuli, such as light irradiation [4, 5], electrochemical gating [6–8], electric field [9–14], mechanical stress [13, 15], and magnetic field [16–18]. As a result, the engineering of diverse functions arising from rational chemical design in molecule junctions allows to realize electronic components from optical switches [4, 5], diodes [19, 20] to transistors [9–14]. Particularly, single-molecule field-effect transistors (FET) have attracted enormous attention because transistors are the fundamental elements of integrated circuits. A significant progress in building and characterizing solid-state single-molecule FETs was achieved in 2009 by Song et al [12]. Their work provided conclusive evidences that solid-state molecular transistors can be realized by tuning the relative alignment of molecular orbital levels with respect to the Fermi level of electrodes by the gate voltage. However, more efforts are still needed to propel the investigation on single-molecule FETs. On the one hand, different types of organic molecules and electrode materials should be explored in order to fabricate molecular transistors with good functional performance, high thermal stability, and high production yield. On the other hand, further investigation on the mechanism underlying the gating effect in single-molecule FETs is also required.

So far, only a few kinds of prototype molecules have been used as the conducting channel of solid-state single-molecule FETs with a back gate or a side gate [12, 14]. In this article, we report the fabrication of single-molecule transistors made from a $\pi$-conjugated benzodifuran (BDF) derivative, a kind of molecule possessing fascinating photophysical and electrochemical properties [21]. Recently, Li et al. demonstrated that the conductance of both thiol- and carbodithiolate-terminated BDFs can be tuned by changing the electrode potentials with respect to an electrochemical reference electrode using the electrochemical gating technique [22]. Their results indicate that BDFs may be good candidates for solid-state single-molecule FETs. However, to realize this goal, the conducting mechanism of BDFs must be understood first. For example, which molecular orbital of BDFs dominates the low-bias junction conductance? How does the gate voltage affect the alignment of molecular orbitals of BDFs

relative to the Fermi level of electrodes? How does the electronic coupling between the BDF molecule and the electrodes depend on the gate voltage? These questions are also essential for all solid-state single-molecule devices. Herein, we address these issues by investigating the electronic transport properties of BDF single-molecule transistors using single-level tunneling model combined with transition voltage spectroscopy (TVS). Our analysis reveals unambiguously that the highest occupied molecular orbital (HOMO) of the thiol-terminated BDF molecule dominates the low-bias junction conductance and that the shift of the HOMO relative to the Fermi level of electrodes caused by the gate voltage is responsible for the modulation of the current through BDF molecules. In contrast, the applied gate voltage only affects slightly the coupling strengths of the HOMO with the gold electrodes.

## Experimental

### Fabrication of device structures

Conventional photolithography and electron beam evaporation (5 nm Ti /40 nm Au) were used to define the macroscopic bonding pads on silicon wafer with 500 nm $SiO_2$. Then, 30 nm Aluminum was deposited and oxidized naturally in air to form $\sim 3-5$ nm $AlO_x$ as dielectric layer. Lastly, a suspending PMMA mask was patterned on PMMA/MMA double layer resist by electron beam lithography (EBL), followed by angle evaporation (20 nm Au without adhesion layer) on the top of $AlO_x$ layer. As a result, $\sim$100 nm wide gold nano constriction was formed on the alumina layer.

### Deposition of molecules and fabrication of molecular junctions

Devices were first cleaned by oxygen plasma to get rid of any organic residue on the electrode surface. Then, the self-assembled monolayer (SAM) of BDF was formed on the gold surface by immersing the sample in 0.1 mM BDF solution in tetrahydrofuran (THF). To keep the molecules from oxidation in air, an argon environment was used for the self-assembly process. Normally, we immersed the devices in the dilute BDF solution overnight to ensure the formation of dense SAM. Subsequently, devices were rinsed in pure THF and blew dry with nitrogen gun. Immediately after this, devices were wire bonded and transferred to the low temperature cryostat. The device was mounted on the sample holder in a vacuum chamber (<5E-5 mbar). The initial resistance of an as-prepared device was measured at low bias ($\pm$50 mV). **Then, feedback controlled electromigration (FCE) was performed**

**to generate a nanogap in the gold nanowire of each device at 4.2 K. During FCE, a bias ramping with the ramping rate of 4 mV/s was applied. As far as 2% conductance decrease was observed, the bias voltage was retracted by 20%. A new reference conductance value was set and the voltage ramping was restarted. The voltage ramping cycles were performed until a target conductance (∼30 kΩ) was reached.**

**Electronic measurements**

We measured current-voltage ($I$-$V$) curves of devices during electromigration in a cryostat (Oxford Ins., OptistatAC-V). The $I$-$V$ curves were measured using a data acquisition board (National Instruments, PCI 6281) together with a homemade LabVIEW program. A current amplifier (Keithley 428) was used to convert the current to voltage. The temperature of device was controlled by the temperature controller (ITC, Model 503). The inelastic electron tunneling (IET) spectrum was measured using a Lock-in amplifier (Stanford Research Systems 830) with an AC modulation of 9 mV at 77.77 Hz.All the devices were characterized by SEM (FEI Quanta 600) after electronic measurements.

**Results and discussion**

Figure 1(a) shows the schematic of a BDF single-molecule FET. One BDF molecule bridges source and drain electrodes by Au-S bonds. The $AlO_x$/Al beneath the molecule serves as the gate electrode to regulate the current through the BDF molecule. The chemical structure of the thiol-terminated BDF molecule is given in Fig. 1(b). The anchor groups (thiols) at two ends are protected by acetyl groups, which are removed before the self-assembling process. Feedback controlled electromigration technique [9, 23, 24] was used to generate a nano-sized gap in the gold nanowire. Briefly, a dense BDF monolayer was assembled on the surface of the gold nanowire (see Supplementary Information Fig. S1). Then, the gold nanowire was broken by the applied current to create a nanometer-scale gap. The inset of Fig. 1(c) presents the scanning electron microscopy (SEM) image of such a nanogap area. As we can see, a sub-nanometer gap was formed in the center of the constriction. During the breaking process, one or very few BDF molecules bridged the nanogap via the formation of the Au-S bonds, forming the desired BDF device. In our measurements, thirty out of more than two hundred devices showed molecular signals. Four

out of thirty devices showed gating effects. To present the data consistently, the measurement results shown in figures 2, 4, 5, and 6 are from the same device.

We started our studies from the investigation on the *I-V* characteristics of the Au-BDF-Au junctions. Figure 1(c) shows a typical *I-V* curve of such a device. As we can see, the current increases linearly at low bias but then increases rapidly after the bias exceeds 0.4 V. The low-bias conductance can be extracted by linear fitting in the bias range of ±0.1 V. Conductance histogram is constructed from 29 single-molecule devices, as shown in Fig. 1(d). Large variations ($1.5\times10^{-6}$ $G_0$ to $3.0\times10^{-3}$ $G_0$) occur for the conductance of Au-BDF-Au junctions. The most probable value is determined to be 3.09 nS ($4\times10^{-5}$ $G_0$), which is smaller than the conductance measured in scanning tunneling microscopy (STM) breaking junction method ($2.9\times10^{-4}G_0$) [22]. However, the most probable value obtained in our case is still in the distribution range of STM measurements. In the STM measurements, much more curves ($> 400$) were measured and thus more geometric configurations were taken into account. In this sense, we attribute the discrepancy in the most probable conductance value to different junction structures constructed in these two platforms and the counting numbers. **Although more than one BDF molecules may connect the electromigrated nano gap between the two gold electrodes, we still believe that the measured Au-BDF-Au devices should be single-molecule junctions because only one prominent peak is present in the conductance histogram in both our case and the STM measurements[22].** The temperature dependence of the measured *I-V* characteristics verifies that the charge transport through BDF molecular junctions is in the tunneling regime (See Supplementary Information Figure S2).

To validate that the measured *I-V* characteristics indeed originate from charge transport through the BDF molecule rather than some artifacts from adsorbents or anything else, we measured the IET spectra of Au-BDF-Au junctions. IET spectroscopy has been accepted as a valid characterization technique for molecular junctions, which can identify the contact geometry and the molecular conformation through the contributions made by some specific internal vibration modes [19, 25–27]. A lock-in amplifier was utilized to directly measure the second harmonic signal $\mathrm{d}^2I/\mathrm{d}V^2$ with high signal-to-noise ratio (See Experimental).

Figure 2(a) shows a typical IET spectrum of one Au-BDF-Au junction. Most features in the IET spectrum are in good agreement with the experimental infrared (IR) adsorption spectrum **and Raman spectrum** of the thiol-terminated BDF molecule, as shown in

Fig. 2(b). Several prominent peaks in the IET spectrum labeled by short red lines and highlighted by green shadow rectangles are assigned to some specific vibration modes of the BDF molecule. This is done by comparing the peak positions of the IET spectrum with those in the experimental and calculated IR spectra of the BDF molecule (See Supplementary Information Figure S3). Four prominent peaks centered at 138 mV, 196 mV, 274 mV, and 357 mV are assigned to $\nu$(18a), $\nu$(8a) phenyl ring mode, $\nu$(C≡C), and $\nu$(CH2) mode, respectively. Another peak at 294 mV is probably due to the vibration mode of C≡N, which is supposed to be found near the peak of C≡C. We notice that the peak centered at ∼390 mV appearing in the IET spectrum is absent in the IR spectrum. Known from the calculated vibration modes of the BDF molecule, this peak is contributed by the C-H stretching mode of the phenyl ring, which is not active in the IR spectroscopy. This is not a surprising result because no selection rules limit the presence of a particular vibration mode in the IET spectrum. The IET spectrum can be further validated by checking the anti-symmetric feature with respect to the zero-bias point. The IET spectra at both bias polarities show close peak positions despite of difference in peak intensity (See Supplementary Information Figure S3). In addition, we checked the broadening of IET peaks as a function of AC modulation voltage (See Supplementary Information Figure S4) [28]. The full width half maximum (FWHM) of characteristic peaks in IET spectrum broadens with increasing AC modulation voltage, which further validates our IET spectrum measurements. Thus, the presence of some characteristic vibration modes of the BDF molecule in the measured IET spectrum confirms that the BDF molecule is the dominating charge transport pathway.

One can simplify the analysis of low-bias transport properties of molecular junctions by introducing a single-level tunneling model, in which one molecular level with the energy $\epsilon_0$ is assumed to be in contact with the source and drain electrodes with the coupling strengths $\Gamma_L$ and $\Gamma_R$. The current through this model system can be calculated using the Landauer formula,

$$I(V) = \frac{2e}{h} \int_{-\infty}^{+\infty} dE\ T(E,V)[f(E - eV/2) - f(E + eV/2)] \tag{1}$$

where $e$ is electron charge, $h$ Planck's constant, and $f(E)$ the Fermi-Dirac distribution function. $T(E,V)$ is the transmission function depending on energy $E$ and voltage $V$. It can be approximated as a Lorentzian function,

$$T(E,V) = \frac{4\Gamma_L\Gamma_R}{(E - (\epsilon_0 + \left(\frac{\Gamma_L - \Gamma_R}{\Gamma_L + \Gamma_R}\right)\frac{eV}{2}))^2 + (\Gamma_L + \Gamma_R)^2} \tag{2}$$

Thus, the molecular level position $\epsilon_0$ and its coupling to the electrode ($\Gamma_L$, $\Gamma_R$) can be obtained by fitting the measured *I-V* curves with the Landauer formula.

Figure 3(a) shows a typical fitted curve using the single-level tunneling model. Three fitting parameters are 0.82 eV for $\epsilon_0$, 0.93 meV for $\Gamma_L$, and 0.90 meV for $\Gamma_R$. By fitting *I-V* curves of all devices, the level position $\epsilon_0$ data are constructed in a histogram, as shown in Fig. 3(b). The histogram shows a peak at 0.78±0.03 eV. This indicates that the energy difference between the conduction orbital and the Fermi level is 0.78 eV, which is within the bias range of our measurement. It is worth noting that the Lorentzian form of the transmission function is a reasonable assumption for the Au-BDF-Au molecular junctions because the obtained molecular orbital energy is much higher than the 5d states of the uncoordinated Au site (around -1.8 eV) [8, 29].

A deeper insight into the large variations of the junction conductance can be obtained by plotting the correlation of the molecular orbital energy $\epsilon_0$ and its coupling strength ($\Gamma$=$\Gamma_L$+$\Gamma_R$) as a function of the junction conductance (Fig. 3(c) and (d)) [30, 31]. One can intuitively expect that the molecular orbital energy $\epsilon_0$ will dramatically affect the junction conductance due to the well-known fact that the transmission coefficient of a one-dimensional rectangular potential barrier follows $T \sim \exp(-\beta L)$, where $L$ is the barrier width and $\beta$ the decay coefficient proportional to $\sqrt{\epsilon_0}$. However, the correlation coefficient between $\Gamma$ and $G$ is determined to be 0.87 while $\epsilon_0$ shows no explicit dependence on $G$, indicating that the different coupling strengths in Au-BDF-Au molecular junctions are the main factor causing variations in the junction conductance.

The transport measurements through two-terminal BDF devices present a clear evidence on the existence of BDF molecule and its energy alignment relative to the Fermi level of gold electrodes. Furthermore, three-terminal BDF devices with gate electrodes modulating the carrier transport will provide more insight into the underlying transport mechanisms. Here, we investigate the gating effect on the current flow through Au-BDF-Au devices. We find that the low-bias conductance can be significantly modulated by the gate voltage. Figure 4(a) shows representative *I-V* curves of one Au-BDF-Au junction at different gate voltages. The low-bias conductance decreases when the gate voltage sweeps from negative to positive values. For comparison, we performed control experiments on devices without BDF molecules, which did not show any gate modulation effects (See Supplementary Information Figure S5). This implies that the gating effect comes from the BDF molecule. In a typical

BDF transistor, the applied gate voltage swept from -2.0 to 2.0 V to guarantee that the gate leakage is much lower than the tunneling current through the BDF molecule (See Supplementary Information Figure S6). The low-bias conductance is plotted as a function of gate voltage in Fig. 4(b). The conductance decreases monotonically with increasing the gate voltage. The inset of Fig. 4(b) is the corresponding two-dimensional differential conductance stability diagram. The differential conductance is numerically calculated from corresponding $I$-$V$ data.

The influence of the gate voltage on $\epsilon_0$ and $\Gamma$ was also studied by fitting $I$-$V$ curves measured at different gate voltages using the Landauer formula (Eq. 1). Figure 4(c) shows $\epsilon_0$ as a function of the gate voltage. The value of $\epsilon_0$ increases monotonically when the gate voltage is increased, suggesting that increasing gate voltage elevates the energy difference between the tunneling level and the Fermi level of electrodes. Generally, enhancement of positive (negative) gate voltage lowers (elevates) the molecular orbitals (HOMO and LUMO) with respect to the Fermi level of electrodes. In the BDF molecular device, when the gate voltage changes from negative to positive value, the HOMO (LUMO) level shifts away from (towards) the Fermi level of electrodes, resulting in the increase of the energy difference ($\epsilon_0$) for HOMO (decrease for LUMO). Therefore, given a constant HOMO-LUMO gap, the shift trend of $\epsilon_0$ as a function of the gate voltage offers an explicit evidence to identify the dominant transport molecular orbital. Considering that the positive gate voltage lowers both HOMO and LUMO energy levels relative to the Fermi energy level, the charge transport in Au-BDF-Au junctions is dominated by the HOMO. This result agrees with previous thiol-anchored molecular devices [8, 12, 29, 31]. Moreover, the ratio between the shift of $\epsilon_0/e$ and the applied gate voltage $V_G$ is around 40 mV/V. The ratio is defined as the gate efficiency factor, which is 0.04 in our case. **It should be noted that a change in the $V_G$ dependence of the molecular orbital level shift occurs below -1 V. As the HOMO level approaches close to the bias window, it becomes increasingly difficult for the negative gate voltage to further elevate the HOMO level due to the charging effects.**

In contrast to the molecular level position $\epsilon_0$, the coupling strengths $\Gamma_L$ and $\Gamma_R$ do not show a monotonic dependence on the gate voltage. As shown in Fig. 4(d), both $\Gamma_L$ and $\Gamma_R$ in this Au-BDF-Au device reach a minimum at the gate voltage of $\sim$ -1 V. The coupling strength varies between 0.4 meV and 0.6 meV when the gate voltage sweeps in the range

from -2 V to 2 V. The close values of $\Gamma_L$, $\Gamma_R$ indicate that the HOMO of the BDF molecule couples almost symmetrically to the source and drain electrodes. More importantly, the small variation in coupling strength during gate sweeping indicates that the contact resistance remains almost unchanged. This suggests that the conductance modulation originates mainly from the shift of HOMO level with respect to the Fermi level of electrodes.

To further verify the gate modulation mechanism, we employed the technique of transition voltage spectroscopy (TVS) to characterize molecular energy levels in Au-BDF-Au junctions [30–33, 36]. This consists in replotting the $I$-$V$ data in a Fowler-Nordheim (F-N) manner, i.e. as $\ln(I/V^2)$ versus $1/V$. Then a minimum in this plot appears at a characteristic voltage $V_{trans}$. It has been established that the transition voltage $V_{trans}$ is related to the applied bias voltage which promotes a significant spectral weight of the transmission function into the bias window. For molecular devices formed through Au-S bonds, $V_{trans}$ is mainly determined by the HOMO-dominated transmission peak [12, 32, 33].

Figure 5(a) shows the F-N plot of $I$-$V$ curves at different gate voltages. A well-defined minimum appears in each F-N plot for both bias polarities. The shift trend of the inflection in each curve is labeled by a dashed arrow. To show the relationship between $V_{trans}$ and the gate voltage, two-dimensional contour plots of $\mathrm{dln}(I/V^2)/\mathrm{d}(1/V)$ at both negative and positive bias as a function of the gate voltage are illustrated in Fig. 5(b) and (c), respectively. All the minimum points in the F-N plot ($\mathrm{dln}(I/V^2)/\mathrm{d}(1/V) = 0$) are highlighted by the dashed line. The absolute values of both $V_{trans}^-$ and $V_{trans}^+$ shift to lower values as the gate voltage decreases. The transition voltages at both bias polarities are linearly proportional to the gate voltage and the gate efficiency factor is determined to be about 0.035. Therefore, the HOMO level is further confirmed to be the nearest molecular orbital dominating the charge transport through Au-BDF-Au devices.

We do not observe significant differences in the transition voltages for both bias polarities, suggesting that the BDF molecule binds almost symmetrically to the source and drain gold electrodes. The transition voltage at zero gate voltage is determined to be 0.57 V, slightly larger than the molecular level position $\epsilon_0$ (0.46 eV) obtained using the single-level tunneling model. This is consistent with the reported relation between the transition voltage and the molecular level position [34, 35]. Furthermore, it has been reported that the absolute value of $V_{trans}$ provides a strong indication to distinguish molecular junctions from vacuum tunneling junctions [36]. Considering that the average value of $V_{trans}$ is 0.89 V for all

measured two-terminal devices (See Supplementary Information Fig. S7), which is much lower than that (1.3 V−2.5 V) measured for gold-vacuum-gold atomic junctions, we can exclude the possibility of tunneling through vacuum junctions without BDF molecules.

Besides the gating effect on molecular level position, the peak intensity of the IET spectra is also found to be gate voltage dependent, as shown in Fig. 6(a). To compare the intensity enhancement, the amplitude of $d^2I/dV^2$ at different gate voltages is normalized by the corresponding differential conductance. Previous studies have demonstrated that strong coupling between internal vibration mode and molecular level results in resonantly enhanced IET spectra for conjugated molecules [12, 26]. Here, a similar enhancement effect is observed when the gate voltage elevates the HOMO level towards the Fermi level of electrodes. However, all the measured peak intensities are strongly enhanced. Besides the vibrational modes of the phenyl ring, the $CH_2$ stretching mode (∼357 mV) is also significantly enhanced, as shown in Fig. 6(a). Figure 6(b) shows the relative intensity enhancement of normalized tunneling conductance, $\eta = d\sigma/\sigma$ for $\nu$(8a) vibration mode, as a function of the gate voltage. The enhancement can be well described by a theoretical equation [26],

$$\eta = \frac{\delta E^2}{(E_M - \overline{E}_F)^2 + (\Gamma/2)^2} \frac{(\overline{E}_F + \Omega - E_M)^2 - (\Gamma/2)^2}{(\overline{E}_F + \Omega - E_M)^2 + (\Gamma/2)^2} \tag{3}$$

where $\overline{E}_F = E_F - eV$, $E_F$ is the unbiased electrode's Fermi level, $\Omega$ is the energy of the vibration mode. $E_M$ is the conducting molecular orbital, and $\delta E$ represents the electron-phonon coupling strength which quantitatively describes the shift of $E_M$ under the influence of a particular vibration mode. The blue curve in Fig. 6(b) is the fitted result using equation (3) to the peak intensity enhancement data. The good agreement between experimental results and the theory further validates the charge transport mechanism in the molecular junction. $\delta E$ is determined to be 43.8 meV, which is much smaller than the reported value[12], suggesting that the influence of the vibration mode, $\nu$(8a), on the shift of HOMO is weaker in this device. This is not surprising since the value of $\delta E$ depends strongly on the specific nanoscale environment of each device[26].

**Conclusions**

In conclusion, we have successfully fabricated BDF single-molecule FET-like devices using the FCE method and measured their gate-modulated transport properties. The conduc-

tance of Au-BDF-Au junctions is increased when the gate voltage becomes more negative, demonstrating that the HOMO of the thiol-terminated BDF molecule is the dominating conduction orbital. Analysis in the framework of the single-level tunneling model and TVS reveals that the reversible energy shift of the HOMO produced by the applied gate voltage is responsible for the observed conductance modulation. Due to the not well-controllable device structures, the low-bias conductance shows large variations. This is mainly caused by the fluctuations in the coupling strengths between the HOMO and the gold electrodes, rather than the changes of the alignment of the HOMO with respect to the electrodes' Fermi level. IET spectroscopy measurements confirm that the observed $I$-$V$ characteristics indeed originate from single BDF molecules in the junctions. These findings lay a solid foundation for extending the functionalities of BDF molecular devices under other external stimuli such as light irradiation and are also of significant benefit for future investigations on other single-molecule devices.

**Electronic Supplementary Information (ESI) available:** Fabrication procedure of BDF single-molecule transistors (Fig. S1); Temperature dependence of $I$-$V$ characteristics of a BDF single-molecule device (Fig. S2); Assignment of peaks of IET spectra to specific vibration modes (Fig. S3); The broadening of the $\nu$(C-H) peak (∼390 mV, C-H stretch of the phenyl ring) in IET spectra due to the AC modulation (Fig. S4); The $I$-$V$ curves of pristine gold vacuum junctions (without BDF molecules) measured at different gate voltages (Fig. S5); Gate leakage in BDF single-molecule transistors (Fig. S6); Histogram of the transition voltages at two bias polarities for BDF single-molecule devices (Fig. S7). See DOI: 10.1039/b000000x/.

**Acknowledgements** This work was financially supported by the Ministry of Science and Technology of the People's Republic of China (No. 2011CB933001, 2012CB932702, 2013CB933404), and the National Natural Science Foundation of China (No. 61321001). Financial support for this research by the Swiss National Science Foundation (grant no. 200021-147143) and the Sino Swiss Science and Technology Cooperation is gratefully ac-

knowledged.

[1] Cuevas J. C.; Scheer E. Molecular Electronics: An Introduction to Theory and Experiment. (World Scientific, Singapore, 2010).

[2] Tao, N. J. Electron transport in molecular junctions. *Nat. Nanotechnol.* **2006**, *1* (3), 173-181.

[3] Aradhya, S. V.; Venkataraman, L. Single-molecule junctions beyond electronic transport. *Nat. Nanotechnol.* **2013**, *8* (6), 399-410.

[4] Tam, E. S.; Parks, J. J.; Shum, W. W.; Zhong, Y.-W.; Santiago-Berros, M. E. B.; Zheng, X.; Yang, W.; Chan, G. K. L.; Abruña, H. D.; Ralph, D. C. Single-molecule conductance of pyridine-terminated dithienylethene switch molecules. *ACS Nano* **2011**, *5* (6), 5115-5123.

[5] Kim, Y.; Hellmuth, T. J.; Sysoiev, D.; Pauly, F.; Pietsch, T.; Wolf, J.; Erbe, A.; Huhn, T.; Groth, U.; Steiner, U. E.; Scheer, E. Charge transport characteristics of diarylethene photoswitching single-molecule junctions. *Nano Lett.* **2012**, *12* (7), 3736-3742.

[6] Xiao, X.; Nagahara, L. A.; Rawlett, A. M.; Tao, N. Electrochemical gate-controlled conductance of single Oligo(phenylene ethynylene)s. *J. Am. Chem. Soc.* **2005**, *127* (25), 9235-9240.

[7] Díez-Pérez, I.; Li, Z.; Guo, S.; Madden, C.; Huang, H.; Che, Y.; Yang, X.; Zang, L.; Tao, N. Ambipolar transport in an electrochemically gated single-molecule field-effect transistor. *ACS Nano* **2012**, *6* (8), 7044-7052.

[8] Capozzi, B.; Chen, Q.; Darancet, P.; Kotiuga, M.; Buzzeo, M.; Neaton, J. B.; Nuckolls, C.; Venkataraman, L. Tunable charge transport in single-molecule junctions via electrolytic gating. *Nano Lett.* **2014**, *14* (3), 1400-1404.

[9] Park, H.; Park, J.; Lim, A. K. L.; Anderson, E. H.; Alivisatos, A. P.; McEuen, P. L. Nanomechanical oscillations in a single-C-60 transistor. *Nature* **2000**, *407* (6800), 57-60.

[10] Liang, W.; Shores, M.; Bockrath, M.; Long, J.; Park, H. Kondo resonance in a single-molecule transistor. *Nature* **2002**, *417* (6890), 725-729.

[11] Park, J.; Pasupathy, A. N.; Goldsmith, J. I.; Chuang, C.; Yaish, Y.; Petta, J. R.; Rinkoski, M.; Sethna, J. P.; Abruna, H. D.; McEuen, P. L.; Ralph, D. C. Coulomb blockade and the Kondo effect in single-atom transistors. *Nature* **2002**, *417* (6890), 722-725.

[12] Song, H.; Kim, Y.; Jang, Y.; Jeong, H.; Reed, M.; Lee, T. Observation of molecular orbital gating. *Nature* **2009**, *462* (7276), 1039-1043.

[13] Perrin, M. L.; Verzijl, C. J. O.; Martin, C. A.; Shaikh, A. J.; Eelkema, R.; van EschJan, H.; van Ruitenbeek, J. M.; Thijssen, J. M.; van der Zant, H. S. J.; Dulic, D. Large tunable image-charge effects in single-molecule junctions. *Nat. Nanotechnol.* **2013**, *8* (4), 282-287.

[14] Xiang, D.; Jeong, H.; Kim, D.; Lee, T.; Cheng, Y.; Wang, Q.; Mayer, D. Three-terminal single-molecule junctions formed by mechanically controllable break junctions with side gating. *Nano Lett.* **2013**, *13* (6), 2809-2813.

[15] Bruot, C.; Hihath, J.; Tao, N. Mechanically controlled molecular orbital alignment in single molecule junctions. *Nat. Nanotechnol.* **2011**, *7* (1), 35-40.

[16] Heersche, H. B.; de Groot, Z.; Folk, J. A.; van der Zant, H. S. J.; Romeike, C.; Wegewijs, M. R.; Zobbi, L.; Barreca, D.; Tondello, E.; Cornia, A. Electron transport through single Mn12 molecular magnets. *Phys. Rev. Lett.* **2006**, *96* (20), 206801.

[17] Burzurí, E.; Zyazin, A. S.; Cornia, A.; van der Zant, H. S. J. Direct observation of magnetic anisotropy in an individual Fe4 single-molecule magnet. *Phys. Rev. Lett.* **2012**, *109* (14), 147203.

[18] Vincent, R.; Klyatskaya, S.; Ruben, M.; Wernsdorfer, W.; Balestro, F. Electronic read-out of a single nuclear spin using a molecular spin transistor. *Nature* **2012**, *488* (7411), 357-360.

[19] Hihath, J.; Bruot, C.; Nakamura, H.; Asai, Y.; Díez-Pérez, I.; Lee, Y.; Yu, L.; Tao, N. Inelastic transport and low-Bias rectification in a single-molecule diode. *ACS Nano* **2011**, *5* (10), 8331-8339.

[20] Lörtscher, E.; Gotsmann, B.; Lee, Y.; Yu, L.; Rettner, C.; Riel, H. Transport properties of a single-molecule diode. *ACS Nano* **2012**, *6* (6), 4931-4939.

[21] Yi, C.; Blum, C.; Lehmann, M.; Keller, S.; Liu, S.-X.; Frei, G.; Neels, A.; Hauser, J.; Schürch, S.; Decurtins, S. Versatile strategy to access fully functionalized benzodifurans: redox-active chromophores for the construction of extended $\pi$-conjugated materials. *J. Org. Chem.* **2010**, *75* (10), 3350-3357.

[22] Li, Z.; Li, H.; Chen, S.; Froehlich, T.; Yi, C.; Schönenberger, C.; Calame, M.; Decurtins, S.; Liu, S.-X.; Borguet, E. Regulating a benzodifuran single molecule redox switch via electrochemical gating and optimization of molecule/electrode coupling. *J. Am. Chem. Soc.* **2014**, *136* (25), 8867-8870.

[23] Park, H.; Lim, A. K. L.; Alivisatos, A. P.; Park, J.; McEuen, P. L. Fabrication of metallic electrodes with nanometer separation by electromigration. *Appl. Phys. Lett.* **1999**, *75* (2),

301-303.

[24] Strachan, D. R.; Smith, D. E.; Johnston, D. E.; Park, T. H.; Therien, M. J.; Bonnell, D. A.; Johnson, A. T. Controlled fabrication of nanogaps in ambient environment for molecular electronics. *Appl. Phys. Lett.* **2005**, *86* (4), 043109.

[25] Kushmerick, J. G.; Lazorcik, J.; Patterson, C. H.; Shashidhar, R.; Seferos, D. S.; Bazan, G. C. Vibronic contributions to charge transport across molecular junctions. *Nano Lett.* **2004**, *4* (4), 639-642.

[26] Yu, L. H.; Zangmeister, C. D.; Kushmerick, J. G. Origin of discrepancies in inelastic electron tunneling spectra of molecular junctions. *Phys. Rev. Lett.* **2007**, *98* (20), 206803.

[27] Kim, Y.; Pietsch, T.; Erbe, A.; Belzig, W.; Scheer, E. Benzenedithiol: a broad-range single-channel molecular conductor. *Nano Lett.* **2011**, *11* (9), 3734-3738.

[28] Song, H.; Reed, M. A.; Lee, T. Single Molecule Electronic Devices. *Adv. Mater.* **2011**, 23 (14), 1583-1608.

[29] Kim, T.; Darancet, P.; Widawsky, J. R.; Kotiuga, M.; Quek, S. Y.; Neaton, J. B.; Venkataraman, L. Determination of energy level alignment and coupling strength in 4,4-bipyridine single-molecule junctions. *Nano Lett.* **2014**, *14* (2), 794-798.

[30] Guo, S.; Hihath, J.; Díez-Pérez, I.; Tao, N. Measurement and statistical analysis of single-molecule current-voltage characteristics, transition voltage spectroscopy, and tunneling barrier height. *J. Am. Chem. Soc.* **2011**, *133* (47), 19189-19197.

[31] Guo, S.; Zhou, G.; Tao, N. Single molecule conductance, thermopower, and transition voltage. *Nano Lett.* **2013**, *13* (9), 4326-4332.

[32] Beebe, J. M.; Kim, B.; Gadzuk, J. W.; Frisbie, C. D.; Kushmerick, J. G. Transition from direct tunneling to field emission in metal-molecule-metal junctions. *Phys. Rev. Lett.* **2006**, *97* (2), 026801.

[33] Beebe, J. M.; Kim, B.; Frisbie, C. D.; Kushmerick, J. G. Measuring relative barrier heights in molecular electronic junctions with transition voltage spectroscopy. *ACS Nano* **2008**, *2* (5), 827-832.

[34] Bâldea, I. Interpretation of stochastic events in single-molecule measurements of conductance and transition voltage spectroscopy. *J. Am. Chem. Soc.* **2012**, *134* (18), 7958-7962.

[35] Chen, J.; Markussen, T.; Thygesen, K. S. Quantifying transition voltage spectroscopy of molecular junctions: Ab initio calculations. *Phys. Rev. B* **2010**, *82* (12), 121412.

[36] Trouwborst, M. L.; Martin, C. A.; Smit, R. H. M.; Guedon, C. M.; Baart, T. A.; van der Molen, S. J.; van Ruitenbeek, J. M. Transition Voltage Spectroscopy and the Nature of Vacuum Tunneling. *Nano Lett.* **2011**, *11* (2), 614-617.

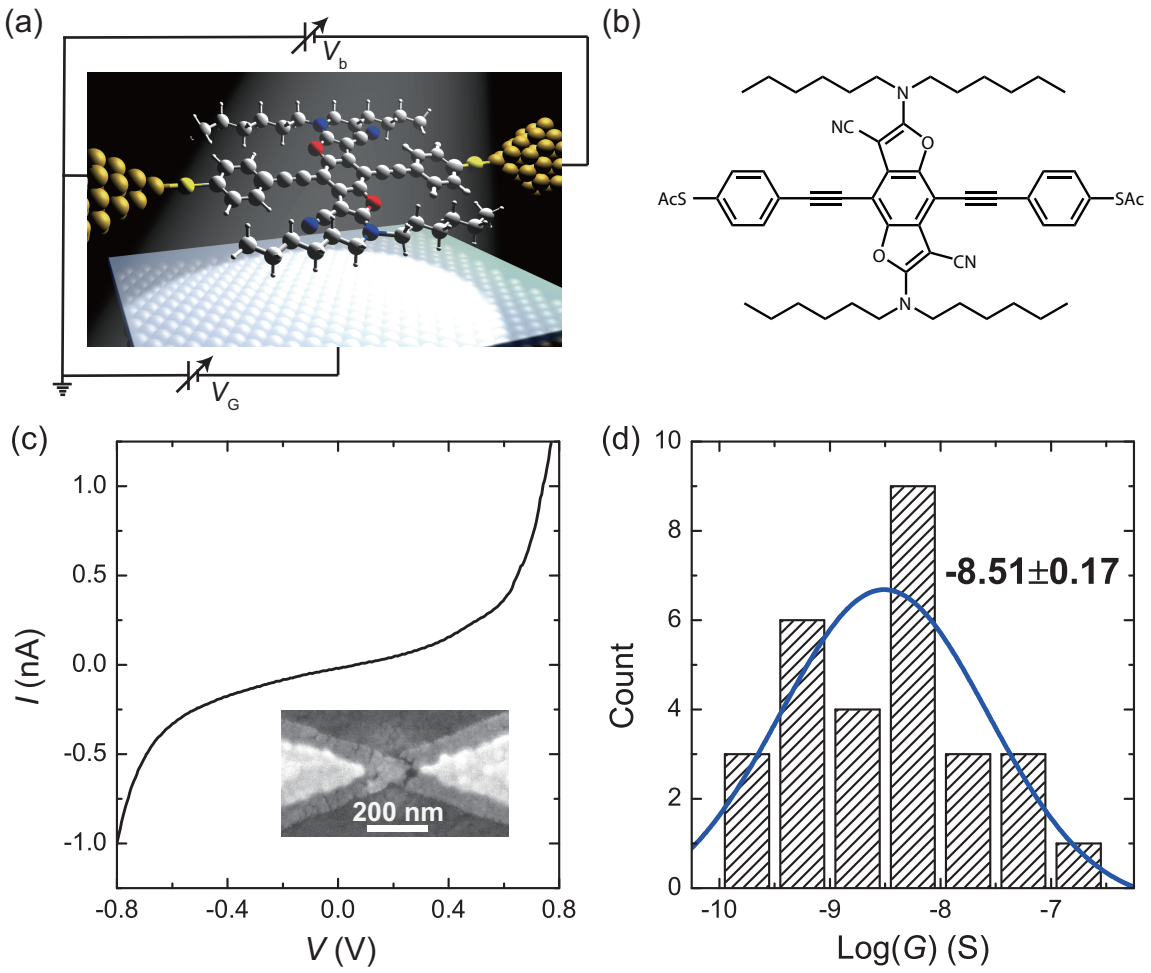


FIG. 1: Single-molecule devices made from BDF molecules fabricated by electromigration technique. **(a)** Schematic of a three-terminal device. The BDF molecule covalently binds to gold nano electrodes through Au-S bonds. A back gate electrode locates beneath the BDF molecule. **(b)** Chemical structure of the BDF derivative. **(c)** Typical *I*-*V* curve for a BDF single-molecule junction. Inset, SEM image of typical device after electromigration and electrical measurements. A nano-sized gap was generated in the center of the gold nanowire. **(d)** Statistic histogram of low-bias conductance values by linear fitting to *I*-*V* curves in the range ±0.1 V. The blue curve represents the gaussian fitting to the histogram. The peak position is -8.51±0.17, corresponding to 3.09 nS.

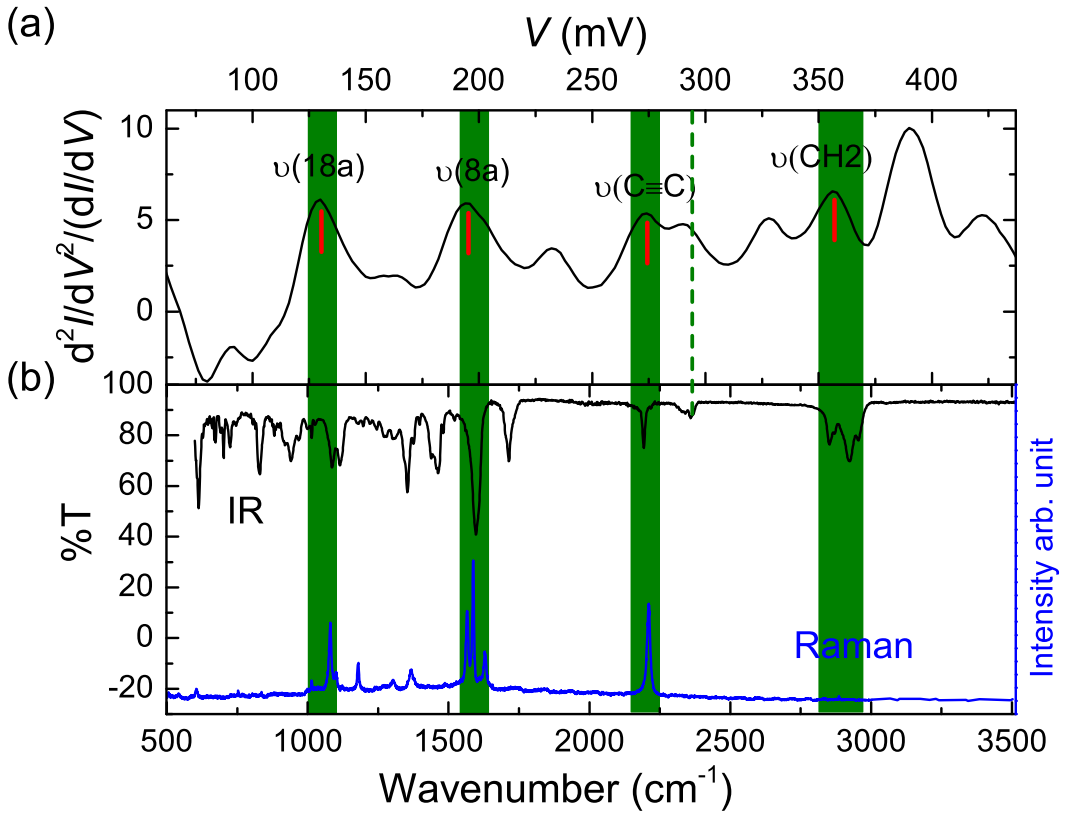


FIG. 2: Assignment of peaks in the IET spectrum of BDF single-molecule devices to different vibration modes. **(a)** Typical IET spectrum for a BDF single-molecule junction measured at 4.2 K. **(b)** Infrared spectrum and Raman spectrum of the BDF molecule. The peaks assigned to specific vibration modes are marked by red vertical lines. The characteristic peaks were highlighted by green shadows in IET spectrum, IR spectrum, and Raman spectrum. The other peak labeled by a green dashed line is also in good agreement with that in the IR spectrum.

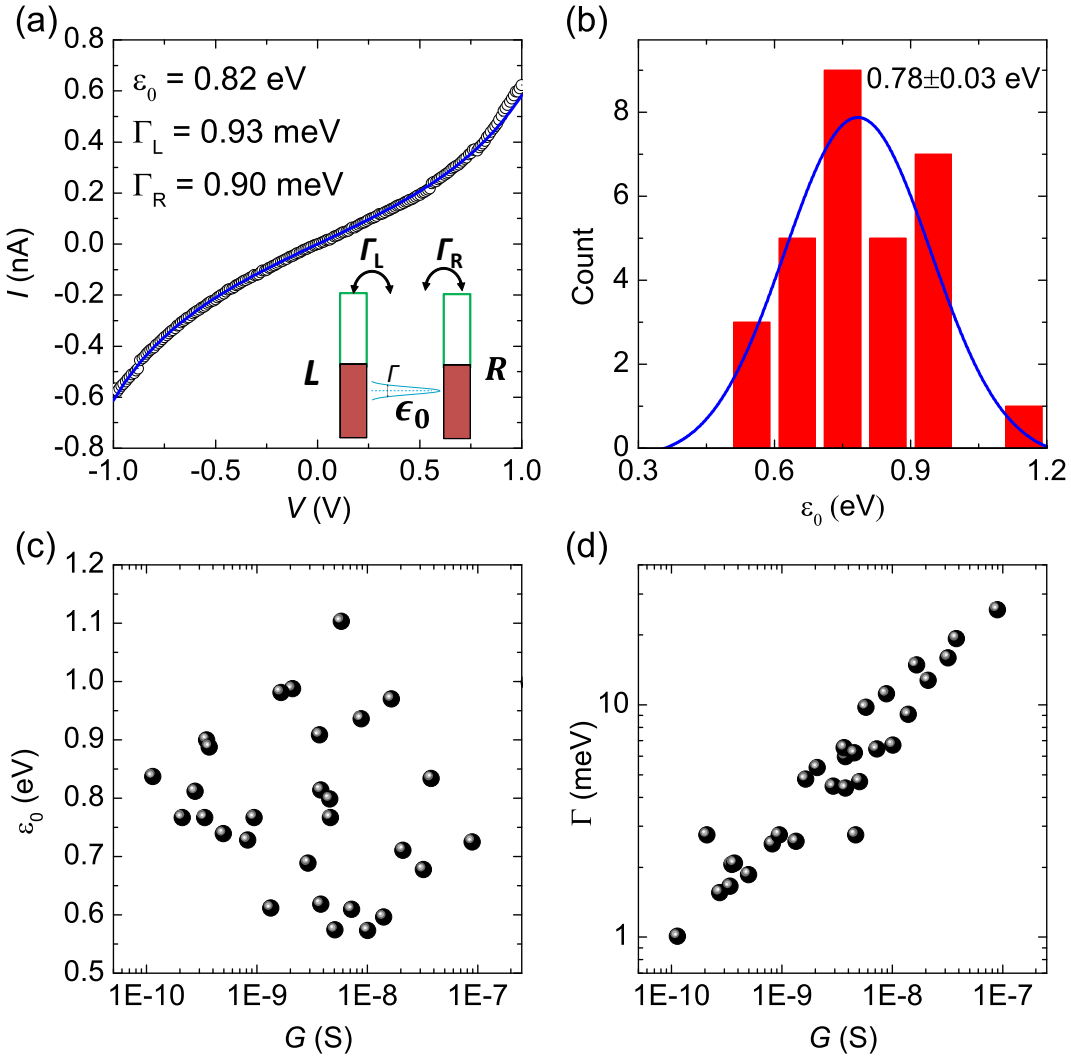


FIG. 3: Analysis of $I$-$V$ curves using the single-level tunneling model. **(a)** Single-level tunneling model fitting (blue curve) to a typical $I$-$V$ curve (black circles). Inset, schematic of single-level tunneling model. A nearest molecular orbital $\epsilon_0$, with coupling strength $\Gamma_L$ and $\Gamma_R$ (level broadening $\Gamma = \Gamma_L + \Gamma_R$), to the left and right electrodes, is responsible for the charge transport. **(b)** Statistic histogram of $\epsilon_0$ extracted by fitting $I$-$V$ curves of all devices. The peak position of gaussian fitting to the histogram is 0.78±0.03 eV. **(c)** Correlation between the molecular level position and the low-bias conductance. The data suggest a low correlation coefficient between $\epsilon_0$ and $G$. **(d)** Correlation between the coupling strength $\Gamma$, and the low-bias conductance $G$. The correlation coefficient is 0.87.

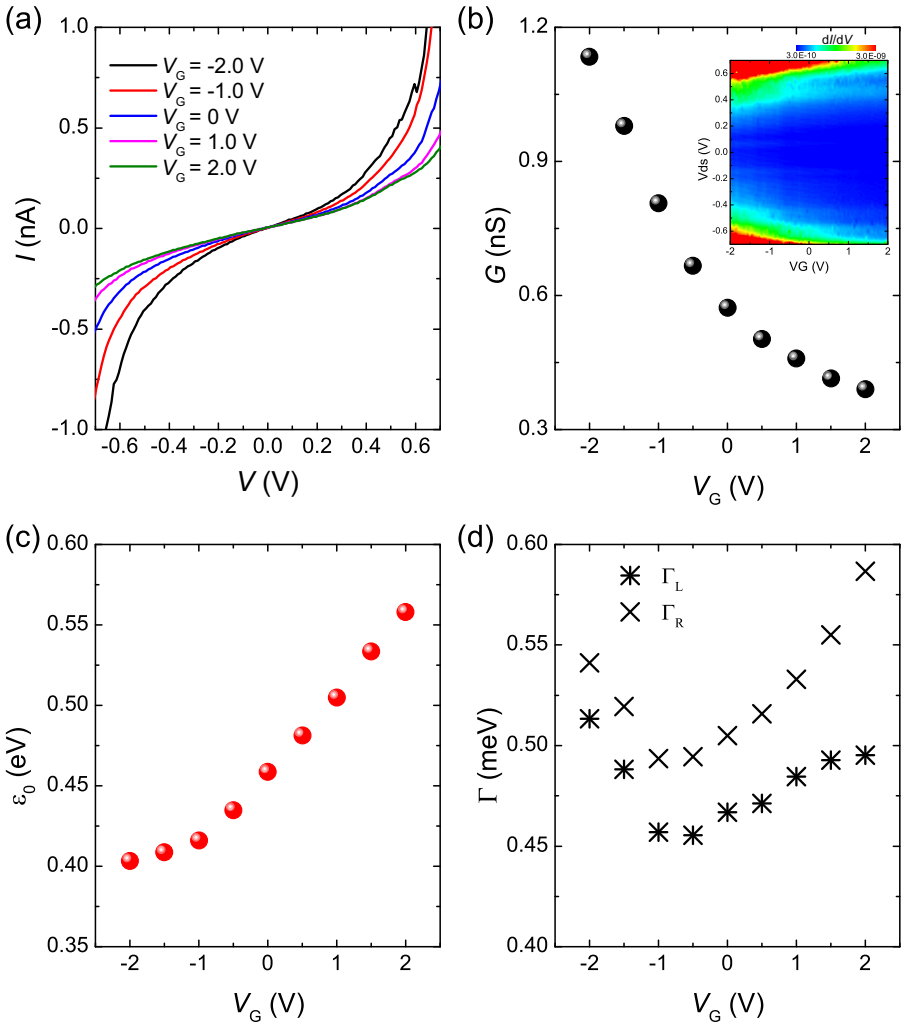


FIG. 4: The gate modulation in BDF single-molecule transistors. **(a)** $I$-$V$ characteristic curves at different gate voltages. **(b)** The low-bias conductance as a function of gate voltage. Inset, the differential conductance (stability diagram) as a function of gate and bias voltage. The differential conductance is numerically calculated from $I$-$V$ curves. **(c)** The $\epsilon_0$ value as a function of gate voltage. **(d)** The influence of the gate voltage on the nearest molecular orbital coupling strength to the left (star) and right (cross) electrodes.

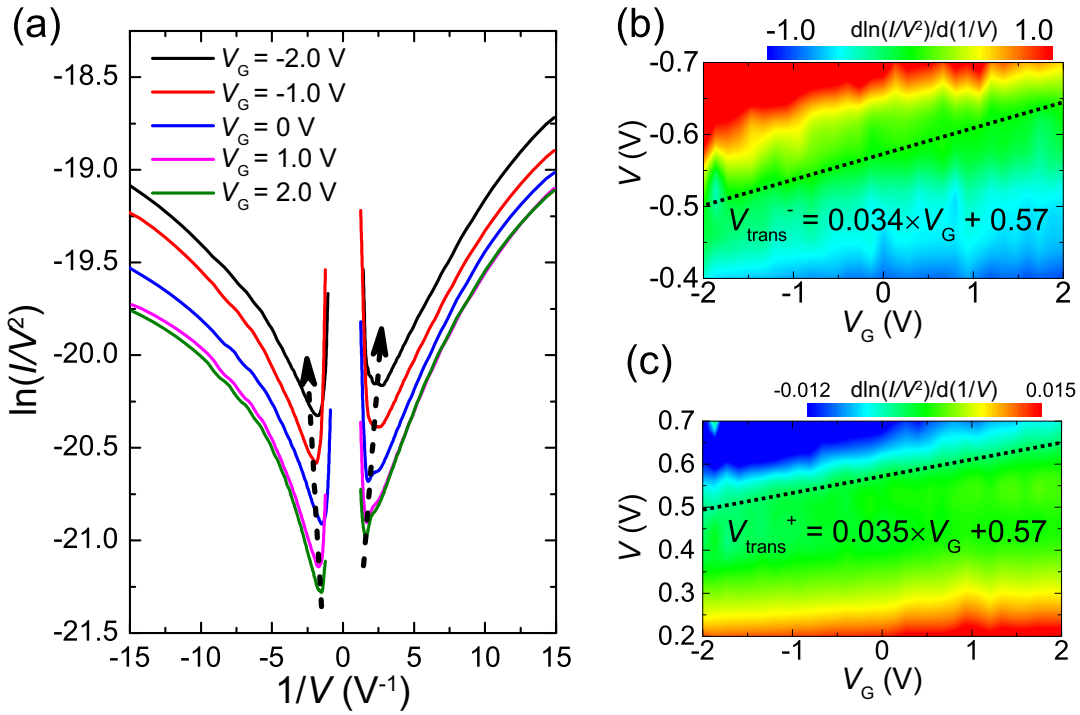


FIG. 5: Transition voltage spectroscopy of BDF molecular devices. **(a)** F-N plot of $I$-$V$ curves at different gate voltages. Two dashed lines mark the shift trend of transition points with the gate voltage in both bias polarities. 2D contour plot $\mathrm{dln}(I/V^2)/\mathrm{d}(1/V)$ at negative **(b)** and positive **(c)** bias as a function of gate and bias voltage. All the minimum points in F-N plot ($\mathrm{dln}(I/V^2)/\mathrm{d}(1/V) = 0$) are highlighted by the dashed line. The transition voltages at both bias polarities are linearly proportional to the gate voltage. The gate coupling efficiency is ∼0.035.

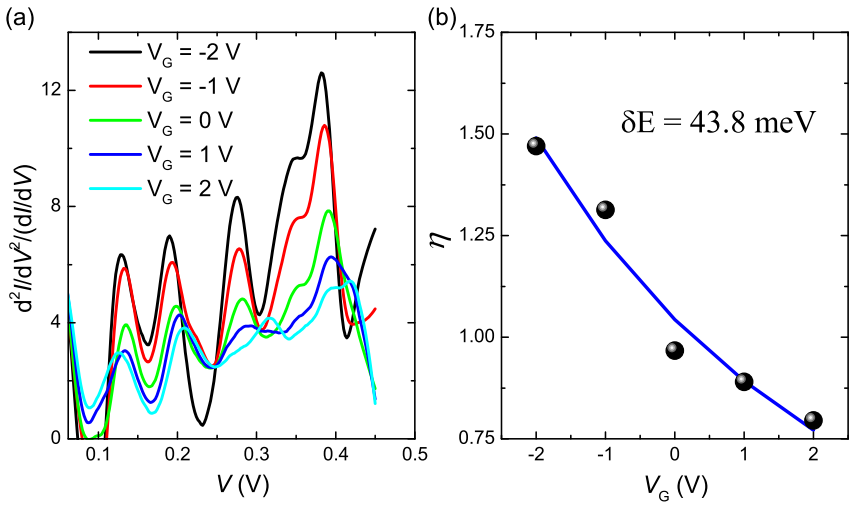


FIG. 6: The influence of the gate voltage on the intensity of IET spectrum. **(a)** Normalized IET spectrum at different gate voltages. The peak intensity is significantly enhanced as the gate voltage shifts from positive to negative values. **(b)** Intensity enhancement (black sphere) for $\nu$(8a) mode in IET spectrum as a function of gate voltage. The blue line shows the fitting curve from the theoretical equation.